

# $\mathcal{PT}$ -Symmetric Quantum Rabi Model

Xilin Lu<sup>1,2,3</sup>, Hui Li<sup>1</sup>, Jia-Kai Shi<sup>1</sup>, Li-Bao Fan<sup>1</sup>, Vladimir Mangazeev<sup>3</sup>, Zi-Min Li<sup>1</sup>,<sup>\*</sup> and Murray T. Batchelor<sup>2</sup>

<sup>1</sup>Hunan Key Laboratory of Nanophotonics and Devices,

Hunan Key Laboratory of Super-Microstructure and Ultrafast Process,

School of Physics and Electronics, Central South University, Changsha 410083, China

<sup>2</sup>Mathematical Science Institute, Australian National University, Canberra ACT 2601, Australia

<sup>3</sup>Research School of Physics, Australian National University, Canberra ACT 2601, Australia

(Dated: April 12, 2023)

In this work, we explore the  $\mathcal{PT}$ -symmetric quantum Rabi model (PTQRM), which describes a  $\mathcal{PT}$ -symmetric qubit coupled to a quantized light field. By employing the adiabatic approximation (AA), we are able to solve this model analytically in the parameter regime of interest and analyze various physical aspects. We investigate the static and dynamic properties of the model, using both the AA and numerical diagonalization. Our analysis reveals a multitude of exceptional points (EPs) that are closely connected with the exactly solvable points in the Hermitian counterpart of the model. Intriguingly, these EPs vanish and revive depending on the light-matter coupling strength. Furthermore, we discuss the time evolution of physical observables under the non-Hermitian Hamiltonian. Our work extends the theory of  $\mathcal{PT}$ -symmetry into the full quantum light-matter interaction regime and provides insights that can be readily enlarged to a broad class of quantum optical systems.

*Introduction.*— Quantum mechanics assumes Hamiltonians that describe physical systems to be Hermitian to ensure that energy eigenvalues are real and the time evolution is unitary. However, there has been a recent surge of interest in non-Hermitian systems [1, 2], especially those with parity-time ( $\mathcal{PT}$ ) symmetry which manifest a transition from purely real to complex conjugate spectra [3].  $\mathcal{PT}$ -symmetry not only is of fundamental importance but also has been applied across myriad fields [4–6].

The  $\mathcal{PT}$ -symmetric qubit, a two-level system with balanced gain and loss, is a paradigmatic model for demonstrating  $\mathcal{PT}$ -symmetry [7]. This simple solvable model effectively reveals the essential consequences of  $\mathcal{PT}$ -symmetry and has been realized across multiple platforms [8, 9]. Further research has explored the interaction between the  $\mathcal{PT}$ -symmetric qubit and classical light fields [10–12], with detailed analyses of energy spectra and phase transitions in these semi-classical models. However,  $\mathcal{PT}$ -symmetry in pure quantum systems, particularly in the context of light-matter interactions, has rarely been visited.

The quantum interaction between light and matter is typically characterized by the quantum Rabi model (QRM), which describes a two-level system coupled to a single-mode quantized light field [13–15]. Despite its simplicity, the QRM exhibits rich physics and has found applications ranging from quantum optics [16] and condensed matter physics [17], to molecular physics and state-of-the-art superconducting circuit quantum electrodynamics [18–20].

Motivated by the QRM, we generalize the theory of  $\mathcal{PT}$ -symmetry into full quantum light-matter interaction systems in this letter. We begin by constructing a  $\mathcal{PT}$ -symmetric Hamiltonian from a realistic physical system and verifying its symmetry. Next, we interpret the model in the displaced oscillator picture and solve it analytically using the adiabatic approximation [21–23]. We

then investigate the static properties, including energy eigenvalues and eigenstates, both analytically and numerically. Interestingly, we observe an infinite number of exceptional points (EPs), which vanish and revive depending on the coupling strength. Additionally, we study the dynamics governed by the non-Hermitian Hamiltonian, with a particular focus on the time evolution of the mean photon number in the cavity.

*Model Hamiltonian.*— The system we propose to study  $\mathcal{PT}$ -symmetry is depicted in Fig. 1(a), in which a non-Hermitian qubit is coupled to a single-mode cavity. This hybrid system can be described by the Hamiltonian

$$H = \frac{\Delta}{2}\sigma_z + \frac{i\epsilon}{2}\sigma_x + \omega a^\dagger a + g\sigma_x(a^\dagger + a), \quad (1)$$

where  $\sigma_{x,z}$  are the spin 1/2 Pauli matrices, with  $\Delta$  being the qubit level splitting and  $\epsilon$  term being the driving or coupling between the two qubit states. The cavity mode with frequency  $\omega$  is governed by the creation and annihilation operators  $a^\dagger$  and  $a$ . The coupling strength between the qubit and the cavity is denoted by  $g$ . Without loss of generality, all system parameters in this work are assumed non-negative.

We begin our symmetry analysis with the non-Hermitian qubit given by

$$H_q^z = \frac{\Delta}{2}\sigma_z + \frac{i\epsilon}{2}\sigma_x. \quad (2)$$

For this non-Hermitian qubit, the parity operator is  $\sigma_x$  and the time reversal operator is the complex conjugate operator [24]. The qubit Hamiltonian remains invariant under the simultaneous parity and time transformations, thus justifying the  $\mathcal{PT}$ -symmetry. The eigenvalues are simply  $\pm\sqrt{\Delta^2 - \epsilon^2}$ , indicating an exceptional point (EP) at  $\epsilon/\Delta = 1$ , where the two eigenvectors coalesce and the eigenvalues become degenerate. When  $\epsilon/\Delta$  crosses the

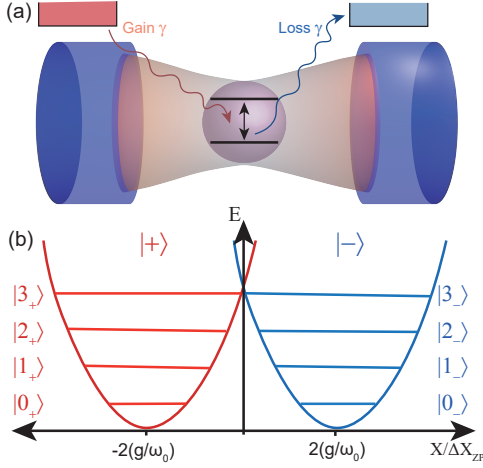


FIG. 1. (a) Schematic of the system consisting of a  $\mathcal{PT}$ -symmetric qubit coupled to a cavity (quantized light field). (b) Displaced oscillator interpretation of the model: two displaced oscillators, one with gain and the other with balanced loss, are coupled by the qubit term  $\frac{\Delta}{2}\sigma_z$ .

EP, the eigenvalues change from real to complex, signaling the phase transition from  $\mathcal{PT}$ -symmetric to  $\mathcal{PT}$ -broken.

For the light field in the cavity, the effects of parity and time operators  $\mathcal{P}$  and  $\mathcal{T}$  are described as  $\mathcal{P} : i \rightarrow i, x \rightarrow -x, p \rightarrow -p$  and  $\mathcal{T} : i \rightarrow -i, x \rightarrow x, p \rightarrow -p$ . It follows that by applying the  $\mathcal{PT}$  transformation to the bosonic creation and annihilation operators, we have  $a \rightarrow -a$  and  $a^\dagger \rightarrow -a^\dagger$ , which is equivalent to the bosonic parity transformation [25].

Therefore, for the hybrid quantum optical system (1), the combined parity operator is given by  $\mathcal{P} = \sigma_z e^{i\pi a^\dagger a}$ , which may be interpreted as the parity of the total excitation number in the system [25]. Meanwhile, the time reversal operation is still to take the complex conjugation. The symmetry of the full Hamiltonian can thus be readily verified as

$$(\mathcal{PT})^\dagger H \mathcal{PT} = H. \quad (3)$$

We thus refer to this system as the  $\mathcal{PT}$ -symmetric quantum Rabi model (PTQRM). Different from the previous approaches which changed the coupling parameter  $g$  of the semi-classical Rabi model into an imaginary value [10–12], here we have taken a more physically intuitive route to obtain the pure quantum model by coupling a  $\mathcal{PT}$ -symmetric qubit to a quantized field.

The PTQRM Hamiltonian (1) reduces to the well-known asymmetric quantum Rabi model (AQRM) if the imaginary term is replaced with the real version  $\frac{\epsilon}{2}\sigma_x$  [14, 26–29]. It further reduces to the standard QRM if  $\epsilon = 0$ .

*Adiabatic approximation.*— From the Hamiltonian (1),

it is clear that the non-Hermiticity of the system originates from the nonzero  $\epsilon$  value. Moreover, the key element for studying non-Hermitian physics of the system is the competition between  $\epsilon$  and  $\Delta$  [4, 7]. As a consequence, the absolute values of  $\Delta/\omega$  and  $\epsilon/\omega$  are not necessarily large. In this case, the precondition of the adiabatic approximation (AA) [22, 23],  $\Delta/\omega < 1$ , remains applicable. Therefore, we can analyze physical phenomena in the PTQRM using the analytic results of the AA [24].

The AA is most physically intuitive in the displaced oscillator picture, where the light-matter interaction is treated as qubit-dependent displacements of the light field [21]. The hybrid system is then mapped to two displaced oscillators coupled to each other, where the coupling is represented by the tunneling between the oscillators described by  $\Delta$  [25]. When  $\Delta/\omega$  is small, only tunnelings within degenerate levels are considered. The basic idea of applying AA to the PTQRM is to include the imaginary term  $\frac{\epsilon}{2}\sigma_x$  as the gain or loss of the two displaced oscillators, as shown in Fig. 1(b). As a consequence, the system Hamiltonian is block-diagonalized into infinitely many  $2 \times 2$  blocks, given by

$$H_n^{\text{AA}} = n\omega - \frac{g^2}{\omega} + \frac{1}{2} \begin{pmatrix} i\epsilon & \Omega_n \\ \Omega_n & -i\epsilon \end{pmatrix}, \quad (4)$$

where

$$\Omega_n = \Delta e^{-2g^2/\omega^2} L_n \left( \frac{4g^2}{\omega^2} \right), \quad (5)$$

with  $L_n(x)$  being the  $n$ th order Laguerre polynomial. Note that the  $2 \times 2$  matrix in Eq. (4) takes the form of a  $\mathcal{PT}$ -symmetric qubit, however with a parameter-dependent driving  $\Omega_n$ , in which the effects of light-matter interaction are incorporated.

The eigenvalues of the PTQRM are obtained by diagonalizing  $H_n$ , giving

$$E_n^\pm = n\omega - \frac{g^2}{\omega} \pm \frac{\sqrt{\Omega_n^2 - \epsilon^2}}{2}. \quad (6)$$

Due to the reduction from the infinite-dimensional  $H$  to the 2-dimensional  $H_n$ , energy levels can be labeled as infinitely many level pairs with the eigenvalues  $E_n^\pm$ . In this work, we start from the zeroth level ( $n = 0$ ). For the  $n$ th level pair, the non-Hermiticity can be seen from the term  $\sqrt{\Omega_n^2 - \epsilon^2}$ , and EPs emerge when  $\epsilon = |\Omega_n|$ .

The corresponding eigenstates are given by

$$|\psi_n^\pm\rangle = \mathcal{N}_n^\pm \begin{pmatrix} \frac{i\epsilon \pm \sqrt{\Omega_n^2 - \epsilon^2}}{\Omega_n} \\ 1 \end{pmatrix}, \quad (7)$$

expressed in the basis  $|n_\pm, \pm\rangle = \exp[\mp g/\omega(a^\dagger - a)] |n\rangle \otimes |\pm x\rangle$ , with  $|n\rangle$  being Fock states and  $\sigma_x |\pm x\rangle = \pm |\pm x\rangle$ .

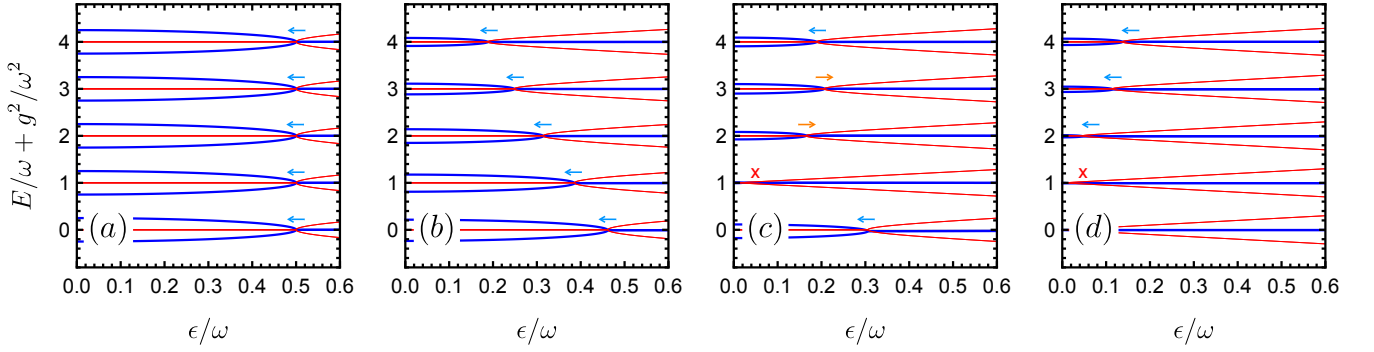


FIG. 2. Vanishing and revival of EPs. (a)-(d) Real (blue thick) and imaginary (red thin) energy spectra of the PTQRM with respect to the qubit parameter  $\epsilon$ , with the coupling strength  $g/\omega = 0, 0.2, 0.5$  and  $1.8$ , respectively. For each figure,  $\Delta/\omega$  is set to be  $0.5$ . For clarity, imaginary parts of eigenvalues have been rescaled by adding level index  $n$ . The arrows in the figures denote the moving directions, blue for vanishing and orange for reviving, of EPs if  $g$  is to be increased.

Here, the normalization factors are calculated as

$$\mathcal{N}_n^\pm = \begin{cases} \frac{1}{\sqrt{2}}, & |\Omega_n| \geq \epsilon, \\ \frac{\Omega_n}{\sqrt{2\epsilon^2 \pm 2\epsilon\sqrt{\epsilon^2 - \Omega_n^2}}}, & |\Omega_n| < \epsilon. \end{cases} \quad (8)$$

When  $\epsilon = 0$ , the above results for the eigensystem revert to the AA for the standard QRM described in Ref. [22].

With the above eigenvalues and eigenstates, analytic expressions for various physical observables can be derived and analyzed.

*Spectrum, exceptional points, and phase transitions.*— In the following, we study the spectral structure and novel non-Hermitian physics of the PTQRM by making use of numerical diagonalization. Meanwhile, we derive analytical AA results to provide us with better physical intuitions. By observing the spectrum, we find a multitude of EPs, whose amount and positions can be deduced from the results of the standard QRM. These EPs are reminiscent of those of the  $\mathcal{PT}$ -symmetric qubits, however with extra modulation owing to the cavity. As we shall see, an exotic effect of the light-matter interaction is the vanishing and revival of EPs.

To observe the interesting EP phenomena under light-matter interaction, we first tune the parameters of the  $\mathcal{PT}$ -symmetric qubit, i.e.,  $\Delta$  and  $\epsilon$ . In the decoupled case, as shown in Fig. 2(a), all level pairs behave the same as the spectrum of the  $\mathcal{PT}$ -symmetric qubit, only with the energy raised by the cavity eigenvalues. All characteristic properties of the  $\mathcal{PT}$ -symmetric qubit are also present. When the coupling strength  $g$  is increased, as in Fig. 2(b)-(d), EPs are shifted due to the interaction, and their overall behavior goes through three stages: vanishing, oscillating revival, and vanishing again. It can be seen from Fig. 2(b) that EPs on higher levels move faster. For small  $g$ , the moving speed appears to depend linearly on the level index  $n$ . As a result, EPs from high

to low vanish in sequence beyond certain values of  $g$ . An interesting effect owing to the light-matter interaction is that EPs may reappear, as shown in Fig. 2(c), where the coupling strength is  $g/\omega = 0.3$ . However, the revival of EPs at this stage is relatively chaotic, in an oscillatory manner. Finally, when the interaction approaches a certain strength, all EPs tend to disappear in sequence, as displayed in Fig. 2(d) with  $g/\omega = 1.8$ .

The vanishing and revival of EPs can be inferred from the PTQRM spectrum with respect to the coupling strength  $g$ , as shown in Fig. 3. We notice that most of the EPs originate from the so-called Juddian points – the level crossings – in the QRM [28]. Juddian points are exactly solvable in the QRM, with their positions and numbers on each pair of energy levels predicted by the defining polynomials [28, 30–33]. In the AQRM, where the  $\epsilon$  term is real, the Juddian points are diabolic points (DPs), also known as conical intersections (CIs), in the three-dimensional parameter space [34, 35]. When the  $\epsilon$  term becomes imaginary, each DP is separated into two

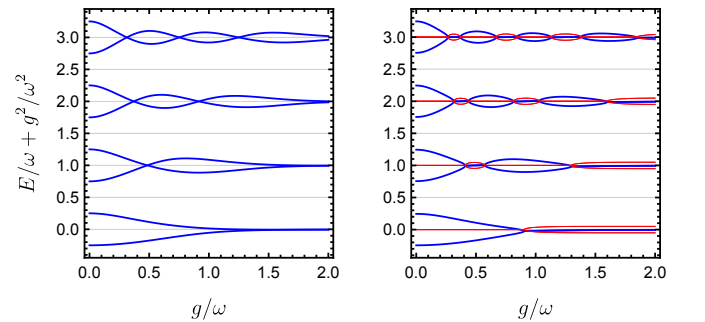


FIG. 3. The energy spectra of the QRM (left) and the PTQRM (right) with respect to the coupling strength  $g$ . The real and imaginary parts of the PTQRM eigenvalues are denoted with blue and red lines, respectively. The parameters are  $\epsilon/\omega = 0.1$  and  $\Delta/\omega = 0.5$ . For clarity, imaginary parts of eigenvalues have been rescaled by adding level index  $n$ .

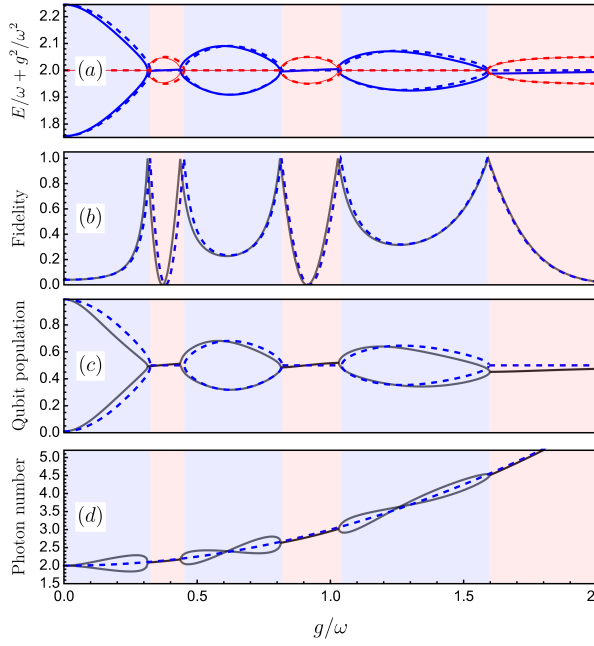


FIG. 4. (a) Real part (blue thick) and imaginary part (red thin) of the energy eigenvalue spectrum with respect to coupling  $g$  for the third pair levels. The imaginary part has been added by 2 for clarity. (b) The fidelity, (c) qubit populations, and (d) mean photon numbers for the corresponding two eigenstates. Relevant parameter values are  $\Delta/\omega = 0.5$  and  $\epsilon/\omega = 0.1$ . Analytic results of AA are depicted in dashed lines. The system is in the  $\mathcal{PT}$ -symmetric phase in the blue regions and the  $\mathcal{PT}$ -broken phase in the red regions.

EPs. Therefore, the number of EPs on each pair of levels is known before some of them vanish [28].

For each level pair, there is an extra EP originating from the infinite coupling limit, irrelevant to the Juddian points. This set of EPs can be understood as formed by the “half” CIs at positive and negative infinity. When this CI goes imaginary, two EPs appear and one goes to finite positive  $g$  while the other goes negative.

Apart from the spectrum, the eigenstates also exhibit novel  $\mathcal{PT}$ -symmetric physics due to light-matter interaction. To explore the eigenstates, we take the second level pair, given by  $H_2$ , as an example. The eigenspectrum together with the corresponding fidelity, qubit population and mean photon number is shown in Fig. 4. Also shown with dashed lines are the results predicted by the analytic expressions of the AA [24]. It is evident that the overall features are satisfactorily captured by the approximation.

The fidelity between states within level pairs exhibits interesting features due to the non-Hermitian nature of the system. In Hermitian systems, eigenstates associated with different eigenvalues are orthogonal. In non-Hermitian systems, however, eigenstates are usually non-orthogonal and even parallel at EPs [24]. The fidelity between two pure states is defined as  $F_{12} = |\langle \psi_1 | \psi_2 \rangle|^2$ . Two

states are orthogonal if  $F_{12} = 0$  and parallel if  $F_{12} = 1$ . We observe from Fig. 4(b) that the two eigenstates are generally not orthogonal, with nonzero fidelity. Notably, the eigenstates are parallel at the multiple EPs, with the fidelity being unity — a characteristic of EPs that does not exist in Hermitian systems. An even more exotic feature here is the existence of some specific points between the EPs where the eigenstates are orthogonal, which is absent in normal non-Hermitian systems. Interestingly, these orthogonal points coincide with the original Juddian points in the standard QRM and their positions are independent of the value of  $\epsilon$ . The emergence of the exotic orthogonal points can also be understood from the perspective of the AA, in which the fidelity is expressed as

$$F_n^{\text{AA}} = \begin{cases} \epsilon^2/\Omega_n^2, & |\Omega_n| \geq \epsilon, \\ \Omega_n^2/\epsilon^2, & |\Omega_n| < \epsilon. \end{cases} \quad (9)$$

In the AA for the standard QRM, Juddian points appear when the Laguerre polynomials in  $\Omega_n$  vanish. Correspondingly, the eigenvectors in Eq. (7) become  $\psi_n^+ = (1, 0)^T$  and  $\psi_n^- = (0, 1)^T$ , which are trivially orthogonal.

The qubit population is displayed in Fig. 4(c), with the analytic expression derived from the AA as

$$W = \frac{(1 + \langle \sigma_z \rangle)}{2} = \begin{cases} \frac{1}{2} \pm \frac{\sqrt{\Omega_n^2 - \epsilon^2}}{2\Delta}, & |\Omega_n| \geq \epsilon, \\ \frac{1}{2}, & |\Omega_n| < \epsilon. \end{cases} \quad (10)$$

The overall behavior of the qubit population is similar to that of the real spectrum, i.e., separate when the eigenvalues are real and degenerate when the energies are complex.

Mean photon numbers are also calculated and displayed in Fig. 4(d), including the comparison with the AA expression

$$\langle a^\dagger a \rangle = n + g^2. \quad (11)$$

The AA deviates from the exact results in Fig. 4(d) when eigenvalues are real, which may be understood via the assumptions of the AA. In the reduced subspace, the photon number is definite for a specific  $n$  and displacement  $g$ , given by Eq. (11). This fact is independent of any other system parameters. Therefore, the deviations in Fig. 4(d) cannot be captured solely by the AA and require the inclusion of higher-order tunneling effects [23].

Due to the non-trivial modulation by the light-matter interaction, there is no standard overall real-to-complex phase transition if all energy levels are considered [3]. For any given parameter values, there are always imaginary eigenvalues if the photon numbers are large enough. However, it is convenient to define “local” phases for separate level pairs of the system eigenstates. To be specific,

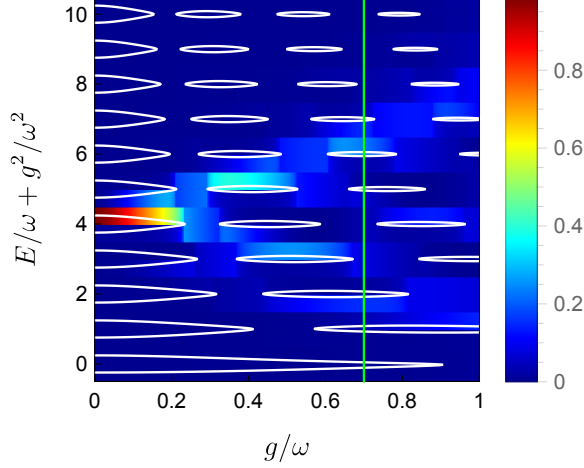


FIG. 5. The real spectrum of the PTQRM with  $\Delta/\omega = 0.5$  and  $\epsilon/\omega = 0.1$ . The background color indicates the mapping of the initial bare state  $|4, +\rangle$  on eigenstates. The vertical green line indicates the coupling strength  $g/\omega = 0.7$ .

for a certain level index  $n$ , we say the system is in the  $\mathcal{PT}$ -symmetric phase if eigenvalues  $E_n^\pm$  are real and the  $\mathcal{PT}$ -broken phase if they are complex. This definition is useful when only a few photons are in the cavity and the Hilbert space is finite-dimensional. The phases are shown in Fig. 4 with blue ( $\mathcal{PT}$ -symmetric) and red ( $\mathcal{PT}$ -broken) backgrounds.

*Dynamics.*— The dynamics of the PTQRM manifest rich physics absent in its Hermitian or semi-classical counterparts. To reveal this, we focus on the time evolution of the mean photon number by numerically solving the time-dependent Schrodinger equation (TDSE). Since the evolution generated by non-Hermitian Hamiltonians does not conserve the norm of the initial state, time-dependent states require renormalization. Therefore, the mean photon number is determined by

$$\langle n \rangle(t) = \langle a^\dagger a \rangle(t) = \frac{\langle \psi(t) | a^\dagger a | \psi(t) \rangle}{\langle \psi(t) | \psi(t) \rangle}, \quad (12)$$

with an initial state  $|\psi(0)\rangle$ .

The dynamics of the mean photon number can be classified into three distinct stages: Firstly, it exhibits oscillations around the initial state; Secondly, it converges towards eigenstates that have the locally largest imaginary eigenvalues; and finally, in the long term, it diverges towards infinite-photon states. The duration of the first two stages is influenced by system parameters and initial states.

In the following, we discuss in detail the case when  $g/\omega = 0.7$  (the vertical line in Fig. 5) as an example, leaving more cases analyzed in Supplemental Material [24]. Fig. 5 illustrates the real eigenvalues of the lowest 22 eigenstates of the PTQRM, with the background

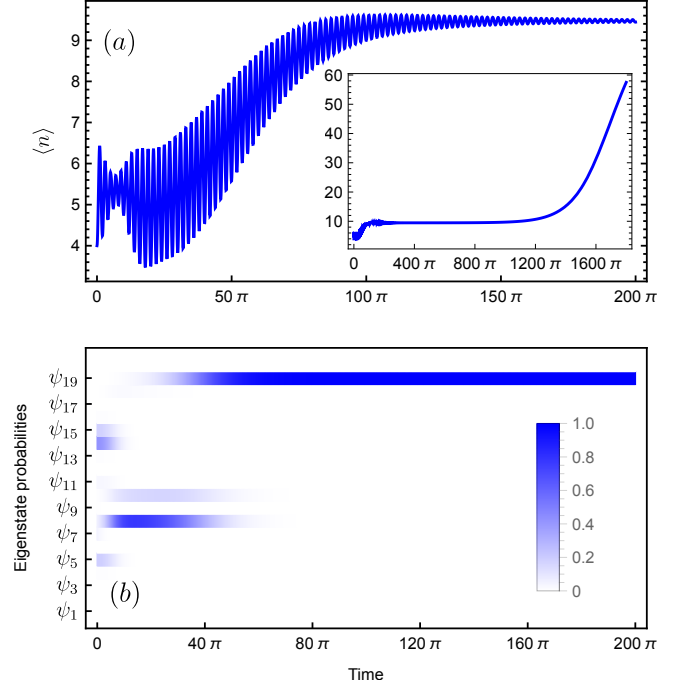


FIG. 6. (a) Time evolution of the photon number with the initial state  $|4, +\rangle$ . The inset is the long-term dynamics where all three stages are present. (b) Time evolution of eigenstate probabilities with the initial state  $|4, +\rangle$ . Parameter values are  $\Delta/\omega = 0.5$ ,  $\epsilon/\omega = 0.1$  and  $g/\omega = 0.7$ .

color being the mapping of the initial bare state  $|4, +\rangle$  on eigenstates. Here, the bare states are  $|n, \pm\rangle = |n\rangle \otimes |\pm z\rangle$ , where  $|n\rangle$  represents the Fock states and  $|\pm z\rangle$  are the eigenstates of  $\sigma_z$ . Eigenstates are denoted as  $|\psi_n\rangle$ , with  $n$  increasing with eigenvalues. By tracing the line  $g/\omega = 0.7$ , we observe that the 3rd, 4th, 8th, 9th, and 10th pairs of eigenstates belong to the  $\mathcal{PT}$ -broken phase. Among them, only the 9th pair is approximately in the middle of two EPs and thus has the largest imaginary energies, as exemplified in Fig. 4.

In Fig. 6(a), we present the time evolution of the mean photon number, starting from the bare state  $|4, +\rangle$ . Initially, the system oscillates around the initial state, but eventually settles into a stable regime where the mean photon number reaches a value of approximately 9. This stable behavior persists for more than 500 cycles before the system finally diverges towards infinite-photon states, as can be observed from the long-term dynamics demonstrated in the inset of the figure.

The transition between the first two stages stands out as particularly interesting. In this process, the imaginary energies  $\text{Im}\{E_n\}$  dictate the growth rates of the corresponding eigenstates  $|\psi_n\rangle$ , even when their probabilities are rather small. As time passes, one eigenstate with the largest imaginary energy prevails through exponential growth. This phenomenon is clearly demonstrated by projecting the bare state  $|4, +\rangle$  onto the eigenstates,



as illustrated in Fig. 5. Notably, even though the initial probability of the dominant eigenstate  $|\psi_{19}\rangle$  is below 0.01, its growth rates still allow it to emerge as the most influential one, as demonstrated in Fig. 6(b).

The 3-stage behavior remains valid even after tuning the system parameters. In particular, an increase in  $\epsilon$  results in a shorter duration of stage 2, while adjusting  $\Delta$  affects the distribution of eigenstate probabilities in the stable regime. Interestingly, the dynamic behavior of the system remains unaffected even when all eigenvalues become complex. By analyzing the imaginary energy landscapes, we observe that the system still converges to the eigenstates with the largest imaginary energies.

In addition to analyzing the evolution with initial conventional Fock states, we investigate the behavior of initial displaced Fock states by varying the displacement amplitudes. Interestingly, we find that although the general dynamics remain similar, the duration of the second stage of evolution increases. Furthermore, our results indicate that the stability of the system is enhanced as the displacement amplitude is increased [24].

The analysis of qubit population dynamics can be conducted in a similar manner, which is elaborated further in the Supplemental Material [24].

While the static properties of the PTQRM can be understood within the AA picture, fitting its dynamic behavior is more challenging. Assuming we choose an initial displaced Fock state  $|n_{\pm}\rangle$ , the state should remain in the subspace with photon number  $n$  for an extended period in the treatment of the AA. In comparison, the numerical data indicates that this is only true when no nearby  $\mathcal{PT}$ -broken states are present. Therefore, the effect of higher-order tunnelings, such as ripples in Fig. 4(d), can be amplified by the growth factor over time in the  $\mathcal{PT}$ -broken phase.

*Summary.*— In this study, we have investigated the  $\mathcal{PT}$ -symmetric quantum Rabi model (PTQRM), which consists of a  $\mathcal{PT}$ -symmetric qubit coupled to a cavity. Focusing on the parameter regime where the interplay between  $\Delta$  and  $\epsilon$  is significant, we have developed an analytical solution based on the adiabatic approximation (AA).

We have discussed the static properties and discovered a multitude of EPs in the spectrum. Each conical intersection in the Hermitian QRM transforms into two EPs of the PTQRM when the  $\epsilon$  term becomes imaginary. Particularly, the energy spectrum exhibits the vanishing and revival of EPs depending on the coupling strength. Based on the eigenstates, we were able to calculate the fidelity, qubit population, and mean photon number. We observed exotic points where different eigenstates are orthogonal, a feature that is absent in normal non-Hermitian systems. Interestingly, these orthogonal points coincide with the level crossing points of the Hermitian QRM.

We also analyzed the dynamics governed by the non-

Hermitian Hamiltonian. Particularly, we observed three stages of the evolution of the cavity photon number: oscillation around the initial state, convergence to nearby eigenstates with the largest imaginary energies, and divergence to infinite-photon states.

This work extends the theory of  $\mathcal{PT}$ -symmetry into the full quantum light-matter interaction regime and provides insights that can be readily enlarged to a broad class of quantum optical systems [25, 36, 37]. We anticipate that the PTQRM will be implemented successfully in multiple experimental platforms, including circuit QED [8] and trapped ions [9], among others.

*Acknowledgements.*— This work is supported by the National Natural Science Foundation of China Grant No. 12205383, the Natural Science Foundation of Changsha Grant No. kq2202082, and Australian Research Council Grant No. DP210102243.

---

\* [zimin.li@csu.edu.cn](mailto:zimin.li@csu.edu.cn)

- [1] N. Moiseyev, *Non-Hermitian Quantum Mechanics* (Cambridge University Press, 2014).
- [2] Y. Ashida, Z. Gong, and M. Ueda, Non-hermitian physics, *Advances in Physics* **69**, 249 (2020).
- [3] C. M. Bender, Introduction to  $\mathcal{PT}$ -symmetric quantum theory, *Contemp. Phys.* **46**, 277 (2005).
- [4] R. El-Ganainy, K. G. Makris, M. Khajavikhan, Z. H. Musslimani, S. Rotter, and D. N. Christodoulides, Non-hermitian physics and PT symmetry, *Nature Physics* **14**, 11 (2018).
- [5] Ş. K. Özdemir, S. Rotter, F. Nori, and L. Yang, Parity-time symmetry and exceptional points in photonics, *Nature Materials* **18**, 783 (2019).
- [6] M.-A. Miri and A. Alù, Exceptional points in optics and photonics, *Science* **363**, 10.1126/science.aar7709 (2019).
- [7] S. Dogra, A. A. Melnikov, and G. S. Paraoanu, Quantum simulation of parity-time symmetry breaking with a superconducting quantum processor, *Commun. Phys.* **4**, 26 (2021).
- [8] M. Naghiloo, M. Abbasi, Y. N. Joglekar, and K. W. Murch, Quantum state tomography across the exceptional point in a single dissipative qubit, *Nature Physics* **15**, 1232 (2019).
- [9] W.-C. Wang, Y.-L. Zhou, H.-L. Zhang, J. Zhang, M.-C. Zhang, Y. Xie, C.-W. Wu, T. Chen, B.-Q. Ou, W. Wu, H. Jing, and P.-X. Chen, Observation of pt-symmetric quantum coherence in a single-ion system, *Physical Review A* **103**, 1020201 (2021).
- [10] Y. N. Joglekar, R. Marathe, P. Durganandini, and R. K. Pathak,  $\mathcal{PT}$  spectroscopy of the Rabi problem, *Phys. Rev. A* **90**, 040101 (2014).
- [11] T. E. Lee and Y. N. Joglekar,  $\mathcal{PT}$ -symmetric Rabi model: Perturbation theory, *Phys. Rev. A* **92**, 042103 (2015).
- [12] Q. Xie, S. Rong, and X. Liu, Exceptional points in a time-periodic parity-time-symmetric Rabi model, *Phys. Rev. A* **98**, 052122 (2018).
- [13] I. I. Rabi, On the process of space quantization, *Phys. Rev.* **49**, 324 (1936).

- [14] D. Braak, Integrability of the Rabi Model, *Phys. Rev. Lett.* **107**, 100401 (2011).
- [15] Q. Xie, H. Zhong, M. T. Batchelor, and C. Lee, The quantum Rabi model: Solution and dynamics, *J. Phys. A: Math. Theor.* **50**, 113001 (2017).
- [16] M. Fox, *Quantum Optics* (Oxford University Press, 2006).
- [17] E. K. Irish, Generalized rotating-wave approximation for arbitrarily large coupling, *Phys. Rev. Lett.* **99**, 173601 (2007).
- [18] P. Forn-Díaz, J. Lisenfeld, D. Marcos, J. J. García-Ripoll, E. Solano, C. J. P. M. Harmans, and J. E. Mooij, Observation of the Bloch-Siegert shift in a qubit-oscillator system in the ultrastrong coupling regime, *Phys. Rev. Lett.* **105**, 237001 (2010).
- [19] F. Yoshihara, T. Fuse, S. Ashhab, K. Kakuyanagi, S. Saito, and K. Semba, Superconducting qubit-oscillator circuit beyond the ultrastrong-coupling regime, *Nat. Phys.* **13**, 44 (2016).
- [20] F. Yoshihara, T. Fuse, Z. Ao, S. Ashhab, K. Kakuyanagi, S. Saito, T. Aoki, K. Koshino, and K. Semba, Inversion of qubit energy levels in qubit-oscillator circuits in the deep-strong-coupling regime, *Phys. Rev. Lett.* **120**, 183601 (2018).
- [21] M. D. Crisp, Application of the displaced oscillator basis in quantum optics, *Phys. Rev. A* **46**, 4138 (1992).
- [22] E. K. Irish, J. Gea-Banacloche, I. Martin, and K. C. Schwab, Dynamics of a two-level system strongly coupled to a high-frequency quantum oscillator, *Phys. Rev. B* **72**, 195410 (2005).
- [23] Z.-M. Li and M. T. Batchelor, Generalized adiabatic approximation to the quantum Rabi model, *Phys. Rev. A* **104**, 033712 (2021).
- [24] See Supplemental Material for further discussions on the  $\mathcal{PT}$ -symmetry, the adiabatic approximation, and more examples of dynamics.
- [25] Z.-M. Li and M. T. Batchelor, Hidden symmetry and tunneling dynamics in asymmetric quantum Rabi models, *Phys. Rev. A* **103**, 023719 (2021).
- [26] Q.-H. Chen, C. Wang, S. He, T. Liu, and K.-L. Wang, Exact solvability of the quantum Rabi model using Bogoliubov operators, *Phys. Rev. A* **86**, 023822 (2012).
- [27] H. Zhong, Q. Xie, X. Guan, M. T. Batchelor, K. Gao, and C. Lee, Analytical energy spectrum for hybrid mechanical systems, *J. Phys. A: Math. Theor.* **47**, 045301 (2014).
- [28] Z.-M. Li and M. T. Batchelor, Algebraic equations for the exceptional eigenspectrum of the generalized Rabi model, *J. Phys. A: Math. Theor.* **48**, 454005 (2015).
- [29] Z.-M. Li and M. T. Batchelor, Addendum to ‘algebraic equations for the exceptional eigenspectrum of the generalized Rabi model’, *J. Phys. A: Math. Theor.* **49**, 369401 (2016).
- [30] B. R. Judd, Exact solutions to a class of Jahn-Teller systems, *J. Phys. C: Solid State Phys.* **12**, 1685 (1979).
- [31] M. Kuš, On the spectrum of a two-level system, *J. Math. Phys.* **26**, 2792 (1985).
- [32] M. Wakayama, Symmetry of asymmetric quantum Rabi models, *J. Phys. A: Math. Theor.* **50**, 174001 (2017).
- [33] K. Kimoto, C. Reyes-Bustos, and M. Wakayama, Determinant expressions of constraint polynomials and the spectrum of the asymmetric quantum Rabi model, *Int. Math. Res. Not.* **2021**, 9458 (2021).
- [34] M. T. Batchelor, Z.-M. Li, and H.-Q. Zhou, Energy landscape and conical intersection points of the driven Rabi model, *J. Phys. A: Math. Theor.* **49**, 01LT01 (2016).
- [35] Z.-M. Li, D. Ferri, D. Tilbrook, and M. T. Batchelor, Generalized adiabatic approximation to the asymmetric quantum Rabi model: conical intersections and geometric phases, *J. Phys. A: Math. Theor.* **54**, 405201 (2021).
- [36] Q.-T. Xie, S. Cui, J.-P. Cao, L. Amico, and H. Fan, Anisotropic Rabi model, *Phys. Rev. X* **4**, 021046 (2014).
- [37] Y.-F. Xie, L. Duan, and Q.-H. Chen, Quantum Rabi-Stark model: solutions and exotic energy spectra, *J. Phys. A: Math. Theor.* **52**, 245304 (2019).

## Supplemental Material: $\mathcal{PT}$ -Symmetric Quantum Rabi Model

### FURTHER DISCUSSIONS ON THE $\mathcal{PT}$ SYMMETRY

The non-Hermitian qubit used in the PTQRM is described by the Hamiltonian

$$H_q^z = \frac{\Delta}{2}\sigma_z + \frac{i\epsilon}{2}\sigma_x = \frac{1}{2} \begin{pmatrix} \Delta & i\epsilon \\ i\epsilon & -\Delta \end{pmatrix}, \quad (S1)$$

where the parity-time symmetry is not immediately apparent. The superscript  $z$  denotes that we are working in a basis with  $\sigma_z$  being diagonal. Therefore, the two states of the qubit are  $|\pm\rangle = |\pm z\rangle$ , with  $\Delta$  representing the level splitting between the two states and  $i\epsilon$  describing the coupling between them.

The imaginary coupling in  $H_q^z$  is not physically intuitive, so it is convenient to rotate the system by performing a unitary transformation generated by

$$U = \frac{1}{\sqrt{2}} \begin{pmatrix} 1 & 1 \\ 1 & -1 \end{pmatrix}, \quad U^\dagger \sigma_x U = \sigma_z, \quad U^\dagger \sigma_z U = \sigma_x. \quad (S2)$$

We then arrive at the new qubit Hamiltonian

$$H_q^x = U^\dagger H_q^z U = \frac{\Delta}{2}\sigma_x + \frac{i\epsilon}{2}\sigma_z = \frac{1}{2} \begin{pmatrix} i\epsilon & \Delta \\ \Delta & -i\epsilon \end{pmatrix}, \quad (S3)$$

where the superscript  $x$  indicates that we are now working in the eigenbasis of  $\sigma_x$ . With  $H_q^x$ , the two states of the qubit are now  $|\pm\rangle = |\pm x\rangle$ , and  $\Delta$  is the coupling between these two states. The diagonal imaginary terms  $i\epsilon$  now indicate the gain of the excited state and the loss of the ground state.

Conventionally, a  $\mathcal{PT}$ -symmetric qubit is expressed in the form of  $H_q^x$  due to the explicit physical interpretation of the imaginary terms [7]. Indeed, it is straightforward to verify the  $H_q^x$  is invariant under the transformation

$$(\mathcal{P}_x \mathcal{T})^\dagger H_q^x (\mathcal{P}_x \mathcal{T}) = H_q^x \quad (\text{S4})$$

with  $\mathcal{P}_x = \sigma_x$  and  $\mathcal{T}$  being the complex conjugation.

To verify the  $\mathcal{PT}$  symmetry of our original qubit Hamiltonian  $H_q^z$ , we only need to rotate everything back into the basis of  $\sigma_z$  by doing the  $U$  transformation again, namely

$$H_q^z = U^\dagger H_q^x U. \quad (\text{S5})$$

As a consequence, the parity operator becomes  $\mathcal{P}_z = \sigma_z$  while the  $\mathcal{T}$  operator remains the same. Finally, the  $\mathcal{PT}$ -symmetry is readily justified, as

$$(\mathcal{P}_z \mathcal{T})^\dagger H_q^z (\mathcal{P}_z \mathcal{T}) = H_q^z. \quad (\text{S6})$$

It is also straightforward to calculate the eigenstates and eigenvalues of  $H_q^z$ . The eigensystem can be divided into two cases depending on the values of  $\Delta$  and  $\epsilon$ , as explained below.

*Case I:*  $\Delta \geq \epsilon$ . The eigenvalues and corresponding eigenstates are

$$E_\pm^z = \pm \frac{1}{2} \sqrt{\Delta^2 - \epsilon^2}, \quad |\psi_\pm^z\rangle = \begin{pmatrix} \frac{-i\Delta \mp i\sqrt{\Delta^2 - \epsilon^2}}{\epsilon} \\ 1 \end{pmatrix}. \quad (\text{S7})$$

It is easy to verify that  $|\psi_\pm^z\rangle$  are also the eigenstates of the combined  $\mathcal{PT}$  operator, namely

$$\mathcal{PT} |\psi_\pm^z\rangle = -|\psi_\pm^z\rangle. \quad (\text{S8})$$

Therefore, the system is in the  $\mathcal{PT}$ -symmetric phase.

*Case II:*  $\Delta < \epsilon$ . The eigenvalues and corresponding eigenstates are

$$E_\pm^z = \pm \frac{i}{2} \sqrt{\epsilon^2 - \Delta^2}, \quad |\psi_\pm^z\rangle = \begin{pmatrix} \frac{-i\Delta \pm \sqrt{\epsilon^2 - \Delta^2}}{\epsilon} \\ 1 \end{pmatrix}, \quad (\text{S9})$$

which now yields

$$\mathcal{PT} |\psi_\pm^z\rangle = \begin{pmatrix} \frac{i\Delta \pm \sqrt{\epsilon^2 - \Delta^2}}{\epsilon} \\ -1 \end{pmatrix} \neq c |\psi_\pm^z\rangle, \quad (c \in \mathbb{C}). \quad (\text{S10})$$

This case is termed as  $\mathcal{PT}$ -broken because the wavefunctions do not have  $\mathcal{PT}$ -symmetry even though the Hamiltonian still commutes with the combined  $\mathcal{PT}$  operator.

## ADIABATIC APPROXIMATION TO THE PTQRM

The Hamiltonian of the PTQRM reads

$$H = \frac{\Delta}{2} \sigma_z + \frac{i\epsilon}{2} \sigma_x + \omega a^\dagger a + g \sigma_x (a^\dagger + a). \quad (\text{S11})$$

To apply the adiabatic approximation (AA), we first introduce the displaced oscillator basis. This is achieved by considering the degenerate qubit limit where  $\Delta = 0$ . In this case, the Hamiltonian becomes

$$H_{\text{do}} = \omega a^\dagger a + g \sigma_x (a^\dagger + a) + \frac{i\epsilon}{2} \sigma_x. \quad (\text{S12})$$



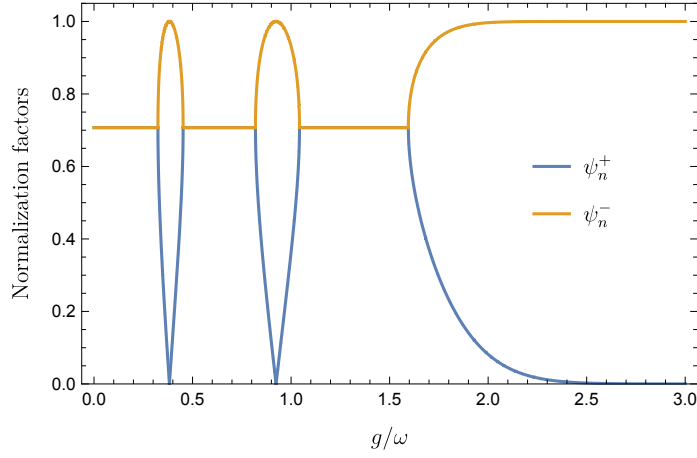


FIG. S1. The normalization factor in Eq. (S18) with respect to the coupling strength  $g/\omega$ .

In the basis of  $|\pm x\rangle$ , where  $\sigma_x |\pm x\rangle = \pm |\pm x\rangle$ , the Hamiltonian can be rewritten in the form of displaced creation and annihilation operators, namely

$$H_{\text{do}}^{\pm} = \omega \left[ \left( a^{\dagger} \pm \frac{g}{\omega} \right) \left( a \pm \frac{g}{\omega} \right) \right] \pm \frac{i\epsilon}{2} - \frac{g^2}{\omega}. \quad (\text{S13})$$

It follows that  $H_{\text{do}}$  is diagonalized by a unitary transformation generated by the position displacement operator  $\mathcal{D}(\alpha) = \exp[-\alpha(a^{\dagger} - a)]$ , with displacement amplitude  $\alpha = \pm g/\omega$  associated with the qubit states. This leads to the solutions

$$\psi_{N,\pm}^{\text{do}} = \mathcal{D}(\pm g) |n\rangle \otimes |\pm x\rangle, \quad E_{N,\pm}^{\text{do}} = n\omega - \frac{g^2}{\omega} \pm \frac{i\epsilon}{2}. \quad (\text{S14})$$

Here  $|n_{\pm}, \pm\rangle = |n_{\pm}\rangle \otimes |\pm x\rangle$  with  $|n_{\pm}\rangle = \mathcal{D}(\pm g/\omega) |n\rangle$  being the displaced Fock states, also known as the generalized or extended coherent states. Intuitively, Eq. (S13) can be interpreted as two displaced harmonic oscillators, with the displacement amplitude  $\pm g/\omega$  and gain or loss rate  $i\epsilon/2$  associated with the qubit states  $|\pm x\rangle$ . This interpretation is known as the displaced oscillator picture and has been extensively used in light-matter interaction models.

Next, we write the QRM Hamiltonian in the basis of displaced oscillator eigenstates (S14) and switch on the parameter  $\Delta$ . The qubit term  $\frac{\Delta}{2}\sigma_z$  couples these eigenstates, which may be understood as the tunneling between the two displaced oscillators. The key assumption of the AA is that only the tunneling process between the eigenstates with the same  $n$  is considered, and higher-order terms are neglected. By doing so, the PTQRM Hamiltonian is decomposed into block-diagonal form, consisting of infinitely many  $2 \times 2$  blocks

$$H_n^{\text{AA}} = n\omega - \frac{g^2}{\omega} + \frac{1}{2} \begin{pmatrix} i\epsilon & \Omega_n \\ \Omega_n & -i\epsilon \end{pmatrix}, \quad (\text{S15})$$

where

$$\Omega_n = \Delta e^{-2g^2/\omega^2} L_n \left( \frac{4g^2}{\omega^2} \right), \quad (\text{S16})$$

with  $L_n(x)$  being the  $n$ th order Laguerre polynomial. Note that the  $2 \times 2$  matrix in Eq. (S15) takes the form of a  $\mathcal{PT}$ -symmetric qubit, however with a parameter-dependent driving  $\Omega_n$ , in which the effects of light-matter interaction are incorporated.

The eigenstates and eigenvalues of Eq. (S15) can be easily solved as

$$E_{n,\pm}^{\text{AA}} = n\omega - \frac{g^2}{\omega} \pm \frac{1}{2} \sqrt{\Omega_n^2 - \epsilon^2}, \quad |\psi_{n,\pm}^{\text{AA}}\rangle = \mathcal{N}_n^{\pm} \begin{pmatrix} \frac{i\epsilon \pm \sqrt{\Omega_n^2 - \epsilon^2}}{\Omega_n} \\ 1 \end{pmatrix}. \quad (\text{S17})$$

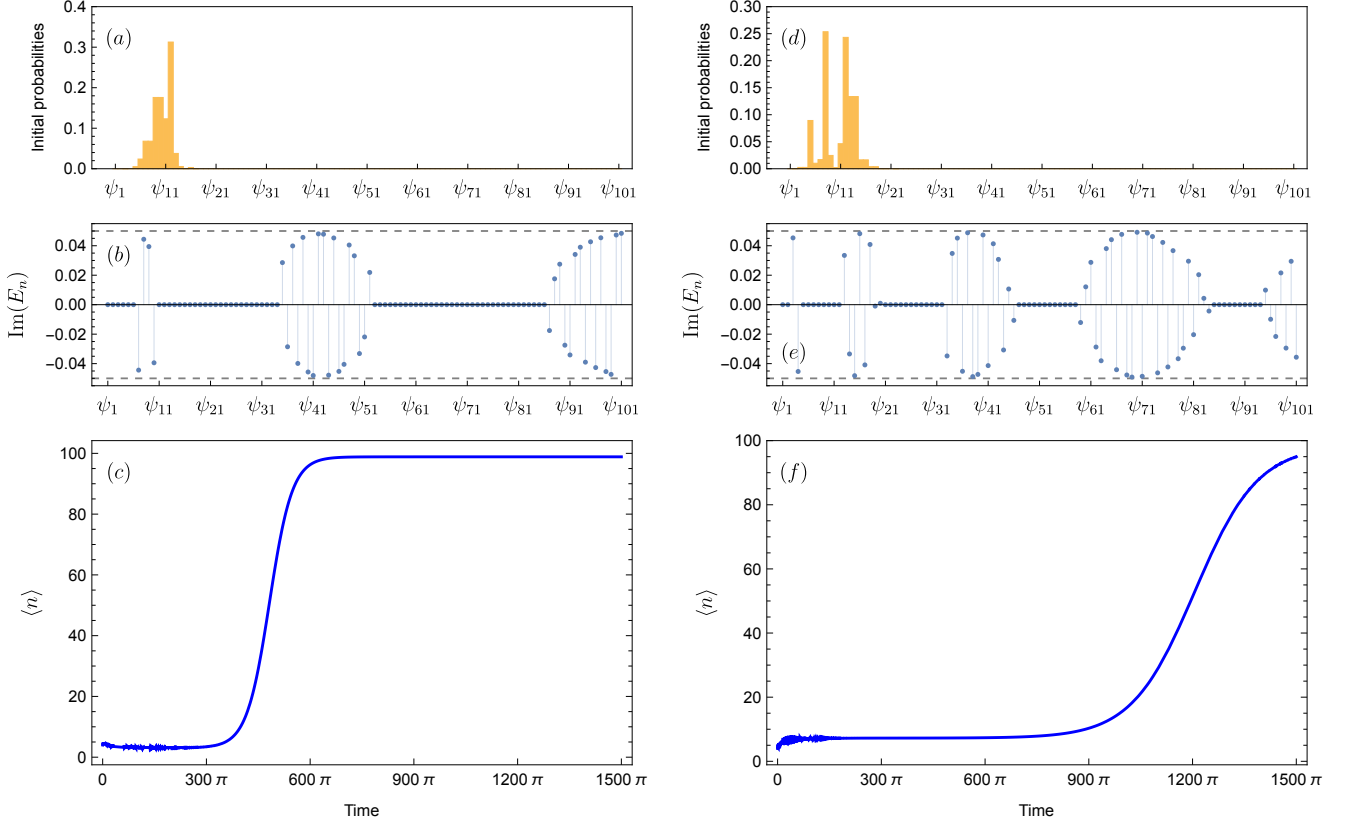


FIG. S2. Further examples of photon dynamics with initial state  $|4, +\rangle$ , and parameters  $\Delta/\omega = 0.5, \epsilon/\omega = 0.1, g/\omega = 0.3$  (a)-(c) and  $g/\omega = 0.5$  (d)-(f). (a)(d) Initial probabilities in the basis of eigenstates, mapped from the initial bare state  $|4, +\rangle$ . (b)(e) Imaginary parts of eigenvalues for the lowest 101 eigenstates, with the dashed grid lines denoting the max and min values  $\pm\epsilon/2$ . (c)(f) Long-term photon dynamics of the system.

The normalization factors  $\mathcal{N}_n^\pm$  are determined by calculating the norm of  $|\psi_n^\pm\rangle$ , which leads to

$$\mathcal{N}_n^\pm = \begin{cases} \frac{1}{\sqrt{2}}, & |\Omega_n| \geq \epsilon \\ \frac{\Omega_n}{\sqrt{2\epsilon^2 \pm 2\epsilon\sqrt{\epsilon^2 - \Omega_n^2}}}, & |\Omega_n| < \epsilon \end{cases}. \quad (\text{S18})$$

The rich physics of  $\mathcal{PT}$ -symmetric quantum light-matter interaction, demonstrated in the main text, can already be observed from the expressions of eigenstates and their normalization factors depicted in Fig. S1.

### FURTHER DISCUSSIONS ON DYNAMICS

In addition to the example provided in the main text, we discuss the dynamics of the other cases  $g/\omega = 0.3, 0.5$  in this section. Moreover, we present further considerations of the effects of tuning the imaginary bias, level splitting, and initial state displacements in the subsequent discussions.

#### *Photon dynamics with various values of $g/\omega$*

To extract information from Fig. 5, we plot the probabilities of the eigenstates and the imaginary eigenvalues for specific values of  $g/\omega$ , as shown in Fig. S2. We consider the lowest 101 eigenstates in our analysis. It's worth noting that even if we consider more eigenstates, the overall dynamics can still be described by the three-stage behavior.

In the case where  $g/\omega = 0.5$ , Fig. 5 in the main text shows the initial probabilities in the eigenstate basis with the initial state  $|4, +\rangle$ , as illustrated in Fig. S2(d). Fig. 5 also reveals the existence of two  $\mathcal{PT}$ -broken eigenstate pairs approximately in the middle of the EPs, specifically the 1st ( $\psi_{3,4}$ ) and the 7th ( $\psi_{15,16}$ ) pairs. The imaginary energies plotted in Fig. S2(e) make this particularly clear, with locally maximal imaginary energies being more prominent in higher-level eigenstates.

Based on the arguments in the main text, the system is expected to converge to one of the eigenstates with locally maximal imaginary energies, depending on which is closer to the initial state. The corresponding photon dynamics are depicted in Fig. S2(f), where we observe that the photon number quickly converges to around 7, indicating the dominance of eigenstate  $\psi_{16}$ . However, after some time ( $t = 1000\pi$ ), the photon number begins to grow to infinity under the non-trivial influence of all higher-level eigenstates with maximal imaginary eigenvalues  $\epsilon/2$ .

In numerical calculations, however, the infinity is unattainable due to the use of a truncated Hilbert space, where the maximal photon number is limited to around 100.

Figs. S2(a)-(c) depict the same behavior when  $g/\omega = 0.3$ .

### Effects of displacements and parameters

Next, we investigate the effects of displacement of the initial state and modifying parameters. We take the case of  $g/\omega = 0.3$  as the example, with the initial state being  $|0, +\rangle$ .

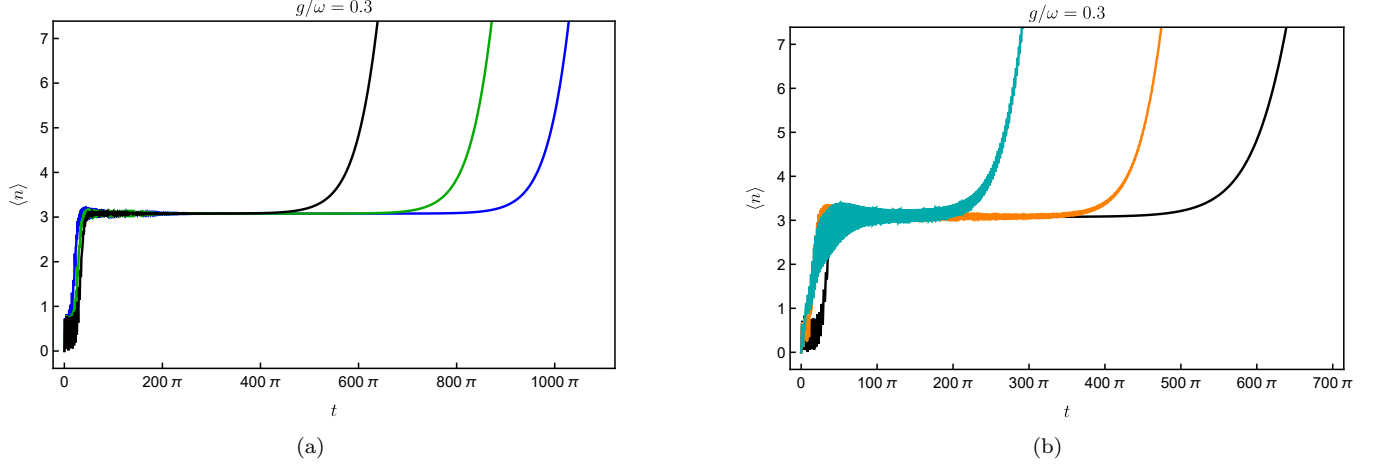


FIG. S3. (a) Mean photon population evolution with displacements: 0 (black),  $g/2\omega$  (green) and  $g/\omega$  (blue) for the initial state  $|0, +\rangle$ ,  $\epsilon/\omega = 0.1$ . (b) Mean photon population evolution with  $\epsilon/\omega = 0.1$  (black), 0.2 (orange) and 0.3 (dark cyan). The initial state is  $|0, +\rangle$ . The black curves are identical in the two plots. The lowest 60 levels are considered, and  $\Delta/\omega = 0.5$  for both plots.

In Fig. S3(a), we displace the initial state with  $\mathcal{D}(g/2\omega)$  and  $\mathcal{D}(g/\omega)$ , displaying their dynamics in green and blue curves, respectively. The non-displaced case is provided in the black curve for reference. We observe that the system stays longer in the eigenstates with a mean photon number of 3 with larger displacement.

If we examine the initial part more closely, where  $t < 50\pi$ , we find that the convergences occur earlier with larger displacement as well. This observation contradicts the explanation by the AA, particularly for the case of displacement  $g/\omega$ , where the system should remain in the subspace with the same mean photon number. Therefore, a more suitable approximation needs to be developed to describe the dynamics of the PTQRM analytically.

The impact of increasing imaginary bias on the dynamics is shown in Fig. S3(b). In contrast to the displacement, the stable time decreases with growing  $\epsilon/\omega$ . Moreover, the oscillation around eigenstates is amplified with the bias as well. Thus, the system stability is diminished.

The effect of splitting, represented by  $\Delta$ , is different from the previous factors. Since the locations of the Juddian points in the QRM depends on  $\Delta$ , by varying it, we deform the imaginary landscape and the system may converge to another eigenstate. For low-lying states, a large modification is required to shift an EP from another level to the current position. In this case, we fix the coupling  $g/\omega = 0.3$  and let  $\Delta/\omega = 1.2$  change the  $\mathcal{PT}$ -broken eigenstate, as shown in Fig. S4(a). In this spectrum, following the grid line  $g/\omega = 0.3$ , we find the only pair of  $\mathcal{PT}$ -broken

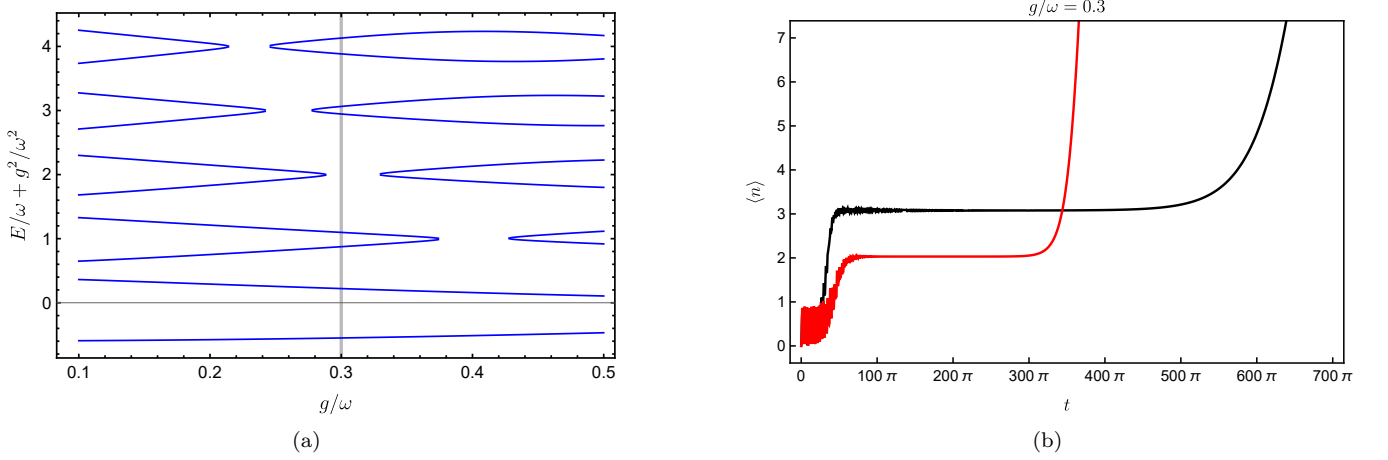


FIG. S4. (a) Real PTQRM spectrum with  $\Delta/\omega = 1.2$ ,  $\epsilon/\omega = 0.1$ . (b) Mean photon population evolution with  $\Delta/\omega = 0.5, 1.2$  in black and red curves, respectively. Initial state  $|0, +\rangle$ ,  $\epsilon/\omega = 0.1$ .

states near initial state  $|0, +\rangle$  contains approximately 2 photons. This aligns with the dynamics shown in Fig. S4(b). Therefore, change in  $\Delta$  may lead to other  $\mathcal{PT}$ -broken eigenstates that the system converges to.

#### Qubit population dynamics

The dynamics of the qubit population are closely related to that of the mean photon population. They oscillate at the same frequency, and  $\langle\sigma_z\rangle$  approaches 0 when the system converges to an eigenstate.

Fig. S5(a) shows the qubit spin behavior for  $g/\omega = 0.7$ . The timing of convergence to a vanishing  $z$ -direction spin component aligns with Fig. 6(a) of the main text, where the photon number  $\langle n \rangle$  stabilizes at around 9.

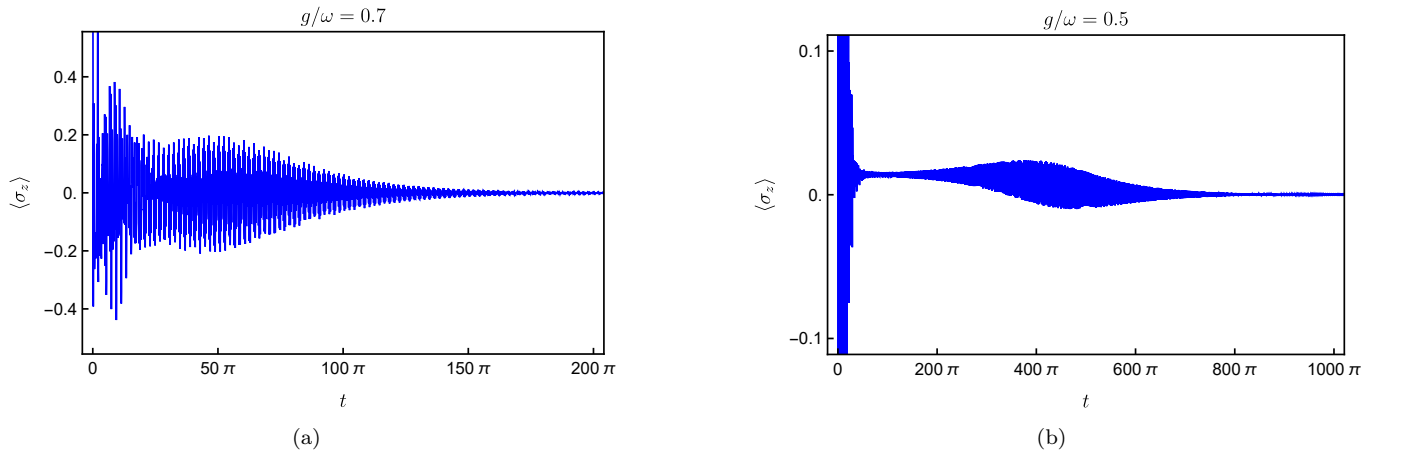


FIG. S5. Qubit population evolution with (a) initial state  $|4, +\rangle$  at  $g/\omega = 0.7$ , (b) initial state  $|2, +\rangle$  at  $g/\omega = 0.5$ . For both plots  $\epsilon/\omega = 0.1$  and  $\Delta/\omega = 0.5$ .

For the case  $g/\omega = 0.5$ , as the system evolves from one eigenstate to another, we expect some ripples from  $t \sim 200\pi$  to  $t \sim 700\pi$  according to Fig. S2(f). This is indeed the case, as shown in Fig. S5(b) (notice the vertical scale). Interestingly, the qubit spin expectation of the eigenstates with  $\langle n \rangle \sim 1$  deviates further from 0 than those with  $\langle n \rangle \sim 7$ . From this observation, we see that larger imaginary energies imply smaller  $|\langle\sigma_z\rangle|$ .

Next, we study the evolution of spin-up components. Fig. S6(a) and Fig. S6(b) show the mean qubit spin and total spin-up contributions with  $g/\omega = 0.1$ . We observe stable oscillations at the beginning for both plots. At this stage, the effects of higher states are negligible, and the qubit behaves as if it is in the  $\mathcal{PT}$ -symmetric phase. Then,

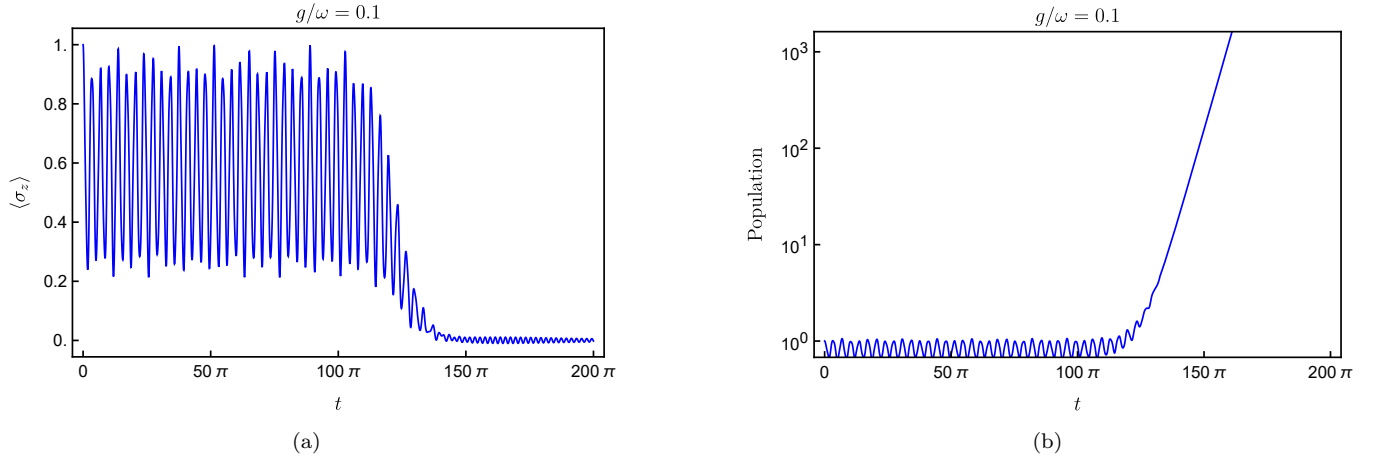


FIG. S6. (a) Expectation value of qubit spin along the  $z$ -direction. (b) The sum of all spin-up contributions. Initial state  $|2, +\rangle$ ,  $\epsilon/\omega = 0.1$  and  $\Delta/\omega = 0.5$ .

after  $t \sim 110\pi$ , the qubit population starts decaying to zero while the total spin-up contribution grows exponentially (linearly in the log plot). The qubit is thus in the  $\mathcal{PT}$ -broken phase. If we choose parameters such that the qubit is initially in the  $\mathcal{PT}$ -broken phase, there will be no oscillating stage, and the dynamics will be very similar to the experimental results reported by Wang *et al.* in [9].